Supporting Information

Lanthanide Metal-organic Frameworks as Multifunctional Sensors for Chemicals and Temperature

Yang Lin[a], Wenxi Zhang[a], Yanjie Lv[a], Yihe Zhao[a], Hongtao Cui[a], Jing Sun[a,*], Xiao Li[a,*], Dongling Zhou[b,*], and Zhongmin Su[a,c]

[a]School of Chemical and Environmental Engineering, Jilin Provincial Science and Technology Innovation Centre of Optical Materials and Chemistry, Jilin Provincial International Joint Research Center of Photo-functional Materials and Chemistry, Changchun University of Science and Technology, Changchun 130022, People's Republic of China.

[b]Department of Chemistry, The University of Hong Kong, Pokfulam Road, Hong Kong, P. R. China.

[c]State Key Laboratory of Supramolecular Structure and Materials, Institute of Theoretical Chemistry, College of Chemistry, Jilin University, Changchun 130021, China.

Email address: Sj-cust@126.com; lix@cust.edu.cn; dlzhou@connect.hku.hk.

Experimental:

Materials and general method: PDAI is based on the literature resultant.[S1] The solvents and other reagents used in this experiment were purchased from Shanghai Aladdin Biochemical Technology Co., Ltd. and were not further purified for use. Characterization of the stability of **CUST-923** and **CUST-924** probes using powder X-ray diffraction (PXRD) and proof of successful synthesis of **CUST-923** and **CUST-924**; Measure the UV absorption spectrum at 200-800 nm using a UV vis spectrophotometer; Using a fluorescence spectrophotometer (Hitachi F7000, Japan) to test the fluorescence spectrum of MOFs during the detection process; Obtaining Fourier transform infrared spectra using an infrared spectrometer (BRUKER VERSEX 70, Germany).

Synthesis of CUST-923: Mix a mixture of $Tb(NO_3)_3·6H_2O$ (0.0227 g, 0.05 mmol), PDAI (0.0246 g, 0.05 mmol), 4 mL DMF, and 2 mL H_2O for 5 minutes, add 8 drops of 3 mol/L HCl solution, then transfer to a stainless steel container lined with polytetrafluoroethylene and seal it. Heat it at 120 ℃ for 72 hours. Cool to room temperature to obtain colorless crystals of **CUST-923**, wash with DMF and distilled water, and dry in air. The molecular formula of **CUST-923** is $C_{23}H_{13}N_3O_{11}Tb$, and the calculated proportion of each element is C: 41.42%; H: 1.95%; N: 6.30%; O: 26.42%. Actual measured value: C: 42.01%; H: 1.71%; N: 6.78%; O: 26.03%.

Synthesis of CUST-924: Using a synthesis method similar to **CUST-923**, the difference is that $Eu(NO_3)_3·6H_2O$(0.0223 g, 0.05 mmol) is used instead of $Tb(NO_3)_3·6H_2O$. Obtain block shaped colorless crystals through filtration, wash with DMF and distilled water, and dry in air. The molecular formula of **CUST-924** is $C_{23}H_{11}EuN_3O_{11}$, and the calculated proportion of each element is C: 41.99%; H: 1.67%; N: 6.39%; O: 26.78%. Actual measurement value: C: 41.36%; H: 1.92%; N: 6.08%; O: 25.99%.

Synthesis of Eu_xTb_{1-x}-PDAI: The preparation process of Eu_xTb_{1-x}-PDAI is similar to **CUST-923**, using a mixture of $Tb(NO_3)_3·6H_2O$ and $Eu(NO_3)_3·6H_2O$ as metal salts, with a total fixed metal salt amount of 0.05 mmol. The ratio of $Tb(NO_3)_3·6H_2O$ to $Eu(NO_3)_3·6H_2O$ varies between 1:9 and 9:1 (Tables. S1).

Cyclic experiment: After the analysis of **CUST-923** and **CUST-924** were detected, **CUST-923** and **CUST-924** were filtered and recovered, washed repeatedly with water, and then dried. Then **CUST-923** and **CUST-924** were used again for analyte detection, and the experimental process was repeated 5 times.

Table S1 The moles ratio of Eu/Tb in compounds produced by ICP.

	The percentage of Eu:Tb in MOFs	The moles analyzed by ICP
$Eu_{0.1}Tb_{0.9}$-PDAI	10% : 90%	0.00532:0.0452
$Eu_{0.2}Tb_{0.8}$-PDAI	20% : 80%	0.0121:0.0441
$Eu_{0.3}Tb_{0.7}$-PDAI	30% : 70%	0.0153:0.0354
$Eu_{0.4}Tb_{0.6}$-PDAI	40% : 60%	0.0234:0.0352
$Eu_{0.5}Tb_{0.5}$-PDAI	50% : 50%	0.0253:0.0256
$Eu_{0.6}Tb_{0.4}$-PDAI	60% : 40%	0.0314:0.023
$Eu_{0.7}Tb_{0.3}$-PDAI	70% : 30%	0.0353:0.0153
$Eu_{0.8}Tb_{0.2}$-PDAI	80% : 20%	0.0433:0.0121
$Eu_{0.9}Tb_{0.1}$-PDAI	90% : 10%	0.0454:0.00511

Table S2 Crystal Data and Structure Refinements for **CUST-923** and **CUST-924**.

	CUST-923	**CUST-924**

Empirical formula	$C_{23}H_{13}N_3O_{11}Tb$	$C_{23}H_{11}EuN_3O_{11}$
Formula weight	666.28	657.31
Temperature/K	298.04	293(2)
Crystal system	monoclinic	monoclinic
Space group	C2/c	C2/c
a/Å	28.4888(14)	28.4963(16)
b/Å	10.0261(4)	10.0575(5)
c/Å	27.1521(13)	27.113(2)
α/°	90	90
β/°	118.885(2)	118.632(2)
γ/°	90	90
Volume/Å^3	6790.6(6)	6820.3(8)
Z	8	8
ρ_{calc}g/cm^3	1.303	1.282
μ/mm^{-1}	2.131	1.887
F(000)	2600.0	2568.0
Reflections collected	43793	24599
Independent reflections	6027	5798
Data/restraints/parameters	6027/6/345	5798/12/353
Goodness-of-fit on F^2	1.076	1.086
Final R indexes [I>=2σ (I)]	R_1 = 0.0390, wR_2 = 0.0942	R_1 = 0.0375, wR_2 = 0.0947
Final R indexes [all data]	R_1 = 0.0536, wR_2 = 0.0996	R_1 = 0.0454, wR_2 = 0.0975

$R_1{}^a=\Sigma||F_o|-|F_c||/\Sigma|F_o|$, $wR_2{}^b=[\Sigma[w(F_o{}^2-F_c{}^2)^2]/\Sigma[w(F_o{}^2)^2]]^{1/2}$

Table S3 Selected bond lengths (Å) for **CUST-923** and **CUST-924**.

Bond	Length/Å	Bond	Length/Å
Tb1-O1	2.266(4)	Tb1-O5	2.336(6)
Tb1-O2[1]	2.389(4)	Tb1-O7[1]	2.515(4)
Tb1-O3[2]	2.423(4)	Tb1-O8[3]	2.415(4)
Tb1-O4[2]	2.401(4)	Tb1-O10[3]	2.412(5)

[1]+X,-Y,-1/2+Z; [2]+X,1-Y,-1/2+Z; [3]1-X,-Y,1-Z; [4]+X,-Y,1/2+Z; [5]+X,1-Y,1/2+Z

Bond	Length/Å	Bond	Length/Å
Eu1-O1[1]	2.371(3)	Eu1-O3	2.419(4)
Eu1-O10[2]	2.369 (4)	Eu1-O9[2]	2.539(4)
Eu1-O7[3]	2.393(3)	Eu1-O4	2.37(3)
Eu1-O8[3]	2.437(4)	Eu1-O11	2.439(6)
Eu1-O4A	2.332(11)		

[1]+X,-Y,-1/2+Z; [2]+X,1-Y,-1/2+Z; [3]1-X,-Y,1-Z; [4]+X,-Y,1/2+Z; [5]+X,1-Y,1/2+Z

Table S4 Selected angles (º) for **CUST-923** and **CUST-924**.

Bond	Angle(˚)	Bond	Angle(˚)
O1-Tb1-O2^{1}	89.01(15)	O4^{2}-Tb1-O7^{1}	166.46(17)
O1-Tb1-O3^{2}	83.92(14)	O4^{2}-Tb1-O8^{3}	81.20(17)
O1-Tb1-O4^{2}	83.37(15)	O4^{2}-Tb1-O10^{3}	111.1(2)
O1-Tb1-O7^{1}	83.09(15)	O8^{3}-Tb1-O3^{2}	133.61(15)
O1-Tb1-O8^{3}	79.88(16)	O8^{3}-Tb1-O7^{1}	96.33(17)
O1-Tb1-O10^{3}	124.50(16)	O10^{3}-Tb1-O3^{2}	148.5(2)
O1-Tb1-O5	161.66(18)	O10^{3}-Tb1-O7^{1}	76.9(2)
O2^{1}-Tb1-O3^{2}	73.94(13)	O10^{3}-Tb1-O8^{3}	52.34(15)
O2^{1}-Tb1-O4^{2}	127.65(14)	O5-Tb1-O2^{1}	84.8(2)
O2^{1}-Tb1-O7^{1}	52.15(13)	O5-Tb1-O3^{2}	77.79(18)
O2^{1}-Tb1-O8^{3}	147.86(18)	O5-Tb1-O4^{2}	86.83(19)
O2^{1}-Tb1-O10^{3}	115.60(18)	O5-Tb1-O7^{1}	106.22(19)
O3^{2}-Tb1-O7^{1}	124.51(13)	O5-Tb1-O8^{3}	113.9(2)
O4^{2}-Tb1-O3^{2}	53.79(13)	O5-Tb1-O10^{3}	73.6(2)

^{1}+X,-Y,-1/2+Z; ^{2}+X,1-Y,-1/2+Z; ^{3}1-X,-Y,1-Z; ^{4}+X,-Y,1/2+Z; ^{5}+X,1-Y,1/2+Z

Bond	Angle(˚)	Bond	Angle(˚)
O1^{1}-Eu1-O7^{2}	87.48(13)	O7^{2}-Eu1-O11	75.38(18)
O1^{1}-Eu1-O8^{2}	82.47(14)	O8^{2}-Eu1-O9^{3}	164.92(16)
O1^{1}-Eu1-O3	75.47(15)	O8^{2}-Eu1-O11	88.4(2)
O1^{1}-Eu1-O9^{3}	82.51(14)	O3-Eu1-O8^{2}	80.22(15)
O1^{1}-Eu1-O11	162.76(17)	O3-Eu1-O9^{3}	97.28(16)
O10^{3}-Eu1-O1^{1}	91.67(14)	O3-Eu1-O11	117.4(2)
O10^{3}-Eu1-O7^{2}	75.25(12)	O4-Eu1-O1^{1}	114.0(14)
O10^{3}-Eu1-O8^{2}	127.40(11)	O11-Eu1-O9^{3}	105.8(2)
O10^{3}-Eu1-O3	148.32(18)	O4-Eu1-O7^{2}	157.2(14)
O10^{3}-Eu1-O9^{3}	51.81(11)	O4-Eu1-O8^{2}	120.0(7)
O10^{3}-Eu1-O11	82.3(2)	O4-Eu1-O3	53.3(10)
O10^{3}-Eu1-O4	110.1(6)	O4-Eu1-O9^{3}	68.0(9)
O7^{2}-Eu1-O8^{2}	52.38(11)	O4-Eu1-O11	83.2(14)
O7^{2}-Eu1-O3	131.52(14)	O4A-Eu1-O3	55.9(3)
O7^{2}-Eu1-O9^{3}	125.47(11)	O4A-Eu1-O11	72.0(7)

^{1}1/2-X,3/2-Y,1-Z; ^{2}1-X,1+Y,3/2-Z; ^{3}1-X,+Y,3/2-Z; ^{4}1-X,-1+Y,3/2-Z

Table S5 MOFs-based fluorescence sensors are used for comparison of the detection of Fe^{3+}.

MOFs	Operation mode	Ksv	LOD (μM)	Ref.
Eu^{3+}/Hoc@UIO-66	Turn-off	1.22×10^{3}	18.0	S2
NIIC-1-Tb	Turn-off	3.83×10^{5}	0.00862	S3
Eu-MOF	Turn-off	8.37×10^{3}	4.32	S4
ZSTU-1	Turn-off	2.69×10^{6}	0.0638	S5
Eu-MOF	Turn-off	2.10×10^{4}	0.027	S6
[Cd(L)(oba)]·0.5DMF}$_n$	Turn-off	4.98×10^{3}	110	S7

CUST-923	Turn-off	1.35×10^4	3.17	This work
CUST-924	Turn-off	7.55×10^3	6.48	This work

Table S6 MOFs-based fluorescence sensors are used for comparison of the detection of $Cr_2O_7^{2-}$.

MOFs	Operation mode	Ksv	LOD (μM)	Ref.
{[Cd(L)-(BPDC)]·2H_2O}$_n$	Turn-off	6.40×10^3	37.6	S8
{[Cd(L)(SDBA)(H_2O)]·0.5H_2O}$_n$	Turn-off	4.97×10^3	48.6	S8
NU-100	Turn-off	1.34×10^4	1.80	S9
{[Zn(L)-(dcdps)]}$_n$	Turn-off	4.46×10^4	10.3	S10
{Zn(L)(bdc)}$_n$	Turn-off	7.72×10^4	5.55	S10
USTS-7	Turn-off	1.31×10^4	2.20	S11
JLNU-10-Eu	Turn-off	4.85×10^3	2.29	S12
CUST-923	Turn-off	8.62×10^3	4.92	This work
CUST-924	Turn-off	5.50×10^3	5.70	This work

Table S7 MOFs-based fluorescence sensors are used for comparison of the detection of CrO_4^{2-}.

MOFs	Operation mode	Ksv	LOD (μM)	Ref.
[Zn(ttz)H_2O]$_n$	Turn-off	2.35×10^3	20	S13
[Cd(2,5-bipi)(5-hip)]$_n$	Turn-off	7.13×10^3	1.68	S14
NH_4[Eu(sal)$_4$(phen)$_2$]	Turn-off	3.60×10^4	0.27	S15
[Zn(IPA)(3-PN)]$_n$	Turn-off	1.00×10^3	18.3	S16
CUST-923	Turn-off	7.39×10^3	5.70	This work
CUST-924	Turn-off	4.67×10^3	10.4	This work

Table S8 MOFs-based fluorescence sensors are used for comparison of the detection of TCH.

MOFs	Operation mode	Ksv	LOD (μM)	Ref.
{[Eu(TATB)(H_2O)]}$_n$	Turn-off	9.06×10^3	4.66	S17
Ag-dcp	Turn-off	3.52×10^4	0.14	S18
CUST-923	Turn-off	1.99×10^4	2.15	This work
CUST-924	Turn-off	1.35×10^4	3.96	This work

Table S9 Reported comparison of MOF thermometer detection performance.

MOFs	Range (K)	Sr (% K^{-1})	Ref.

$Eu_{0.2}Tb_{0.8}L$	40-300	0.15	S19
$Tb_{0.9}Eu_{0.1}$-L	303-423	1.75	S20
$Eu_{0.0143}Tb_{0.9857}$-BDC	298-473	0.28	S21
TbTPTC	313-473	1.05	S22
NIIC-1-Eu	7-200	17	S23
$Eu_{0.1}Tb_{0.9}$-PDAI	303-413	2.3	This work

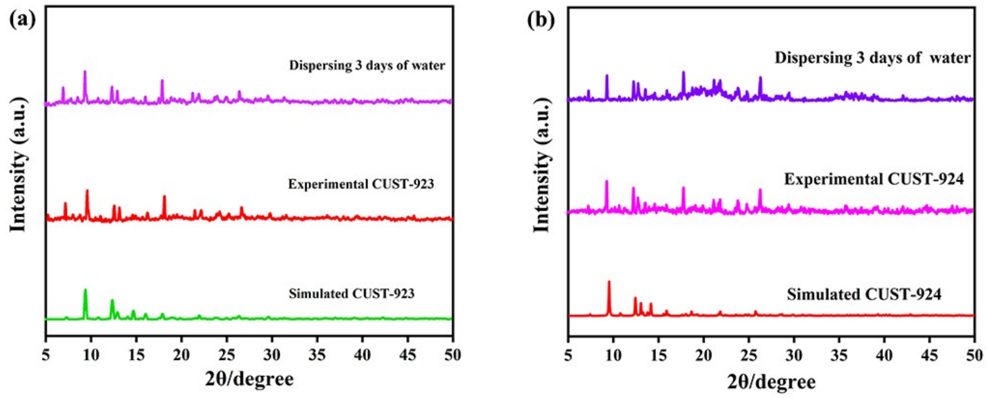

Fig. S1 Powder X-ray diffraction patterns of **CUST-923** and **CUST-924**.

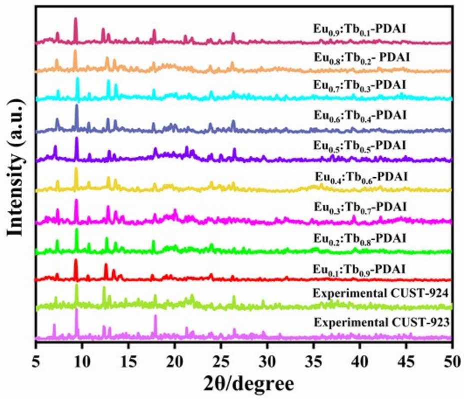

Fig. S2 Powder X-ray diffraction patterns of Eu_xTb_{1-x}-PDAI.

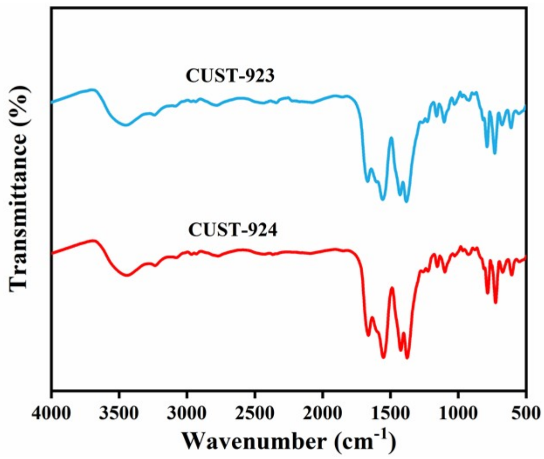

Fig. S3 The IR spectra of CUST-923 and CUST-924.

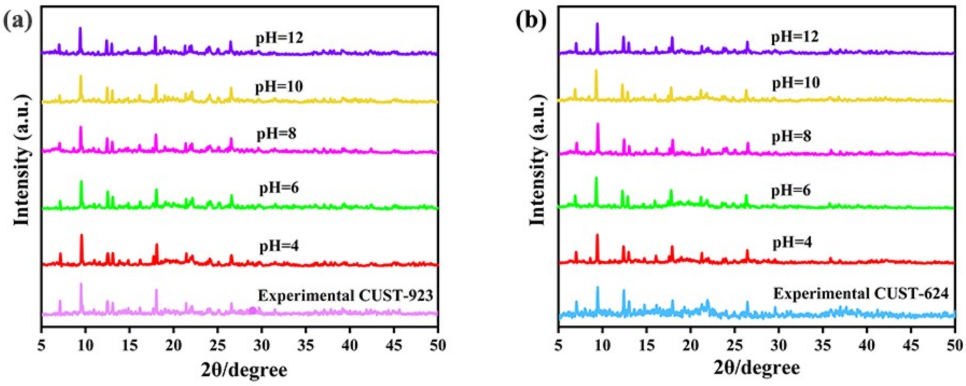

Fig. S4 The PXRD patterns of **CUST-923** and **CUST-924** soaked into aqueous solutions with different pH values.

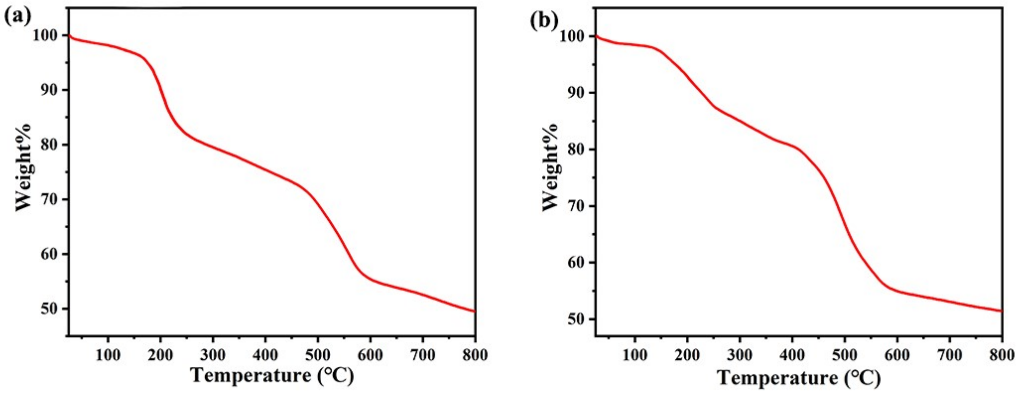

Fig. S5 (a) TGA curves of **CUST-923** and (b) **CUST-924**.

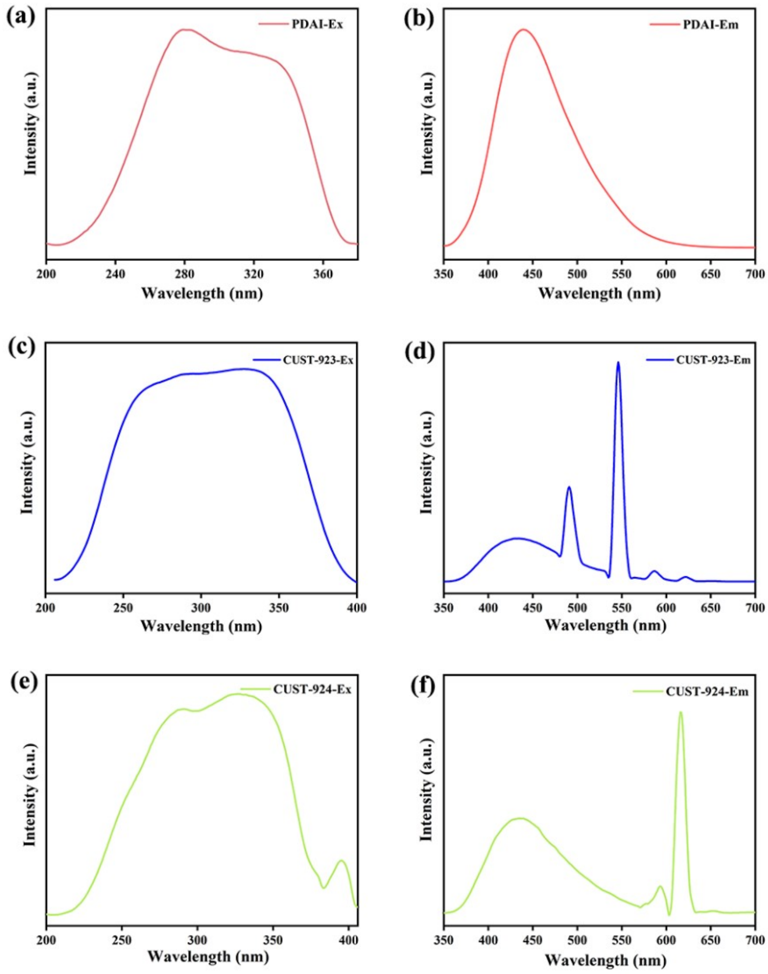

Fig. S6 Solid-state excitation of PDAI (a), **CUST-923** (c) and **CUST-924** (e) and solid-state emission spectra of PDAI (b), **CUST-923** (d) and **CUST-924** (f).

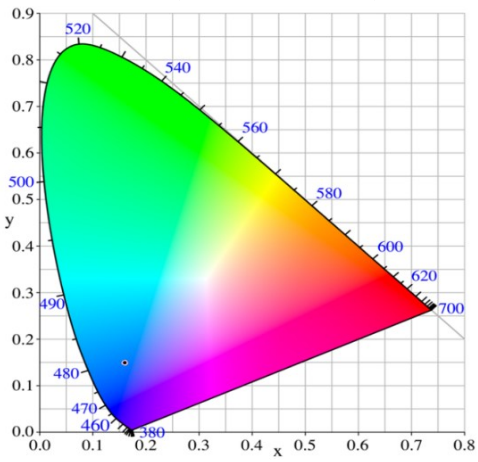

Fig. S7 CIE coordinates for the response of PDAI.

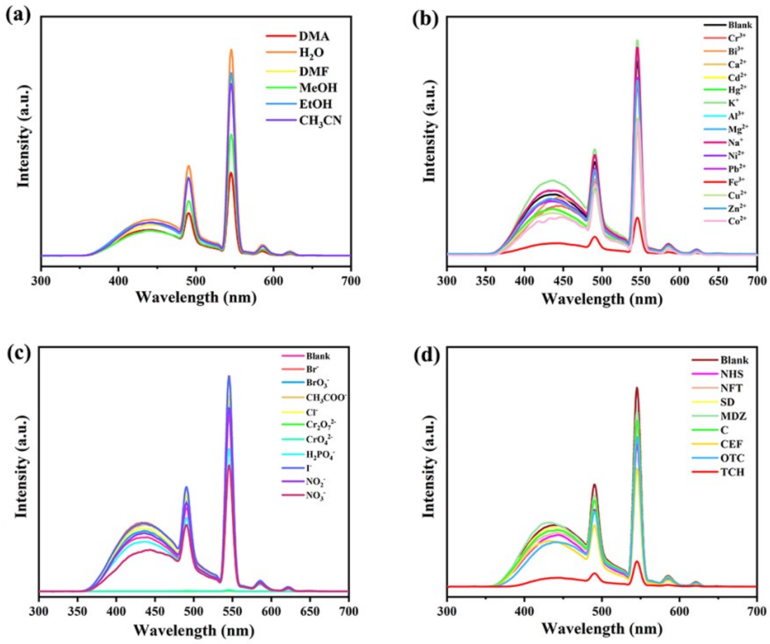

Fig. S8 Emission spectra of **CUST-923** immersed in different solutions: (a) different solvents; (b) Aqueous solution of metal ions; (c) Anions; (d) Antibiotics、

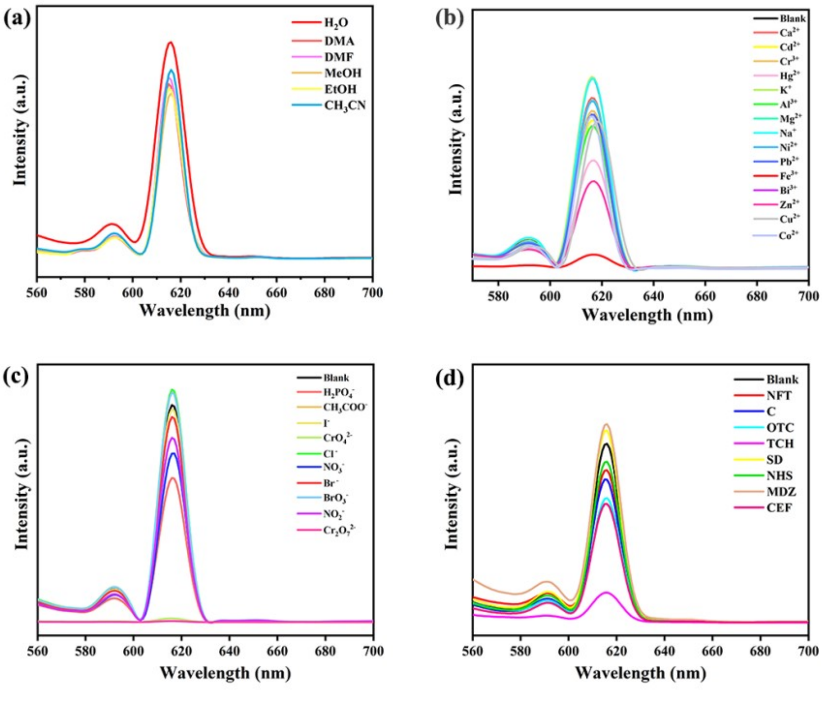

Fig. S9 Emission spectra of **CUST-924** immersed in different solutions: (a) different solvents; (b) Aqueous solution of metal ions; (c) Anions; (d) Antibiotic.

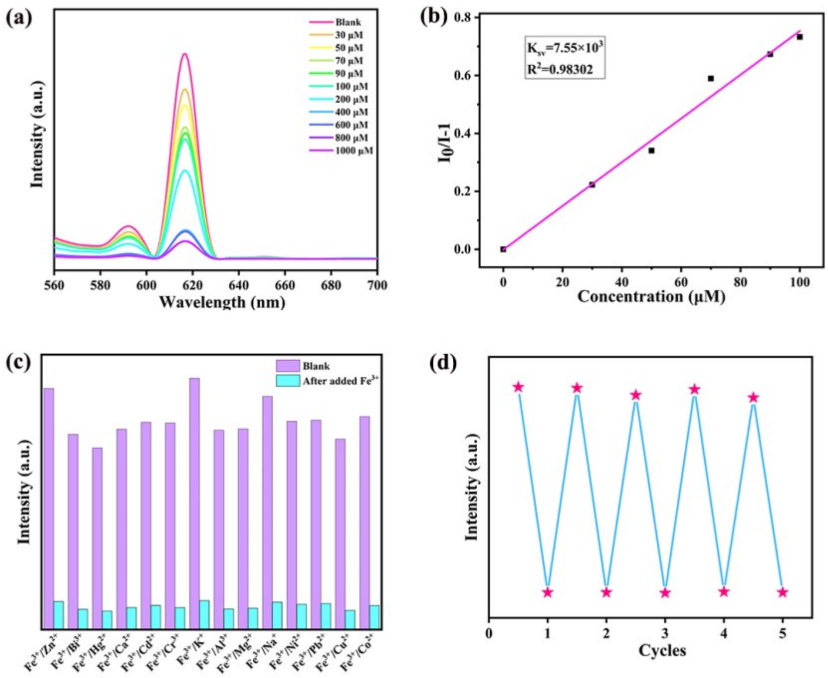

Fig. S10 (a) Concentration-dependent luminescence spectra of **CUST-924** toward Fe^{3+} in aqueous solution. (b) Stern-Volmer plot of **CUST-924** for Fe^{3+}. (c) Anti-interference study of **CUST-924** in water against Fe^{3+} in the presence of different cations. (d) The recyclability test of **CUST-924** after sensing Fe^{3+}.

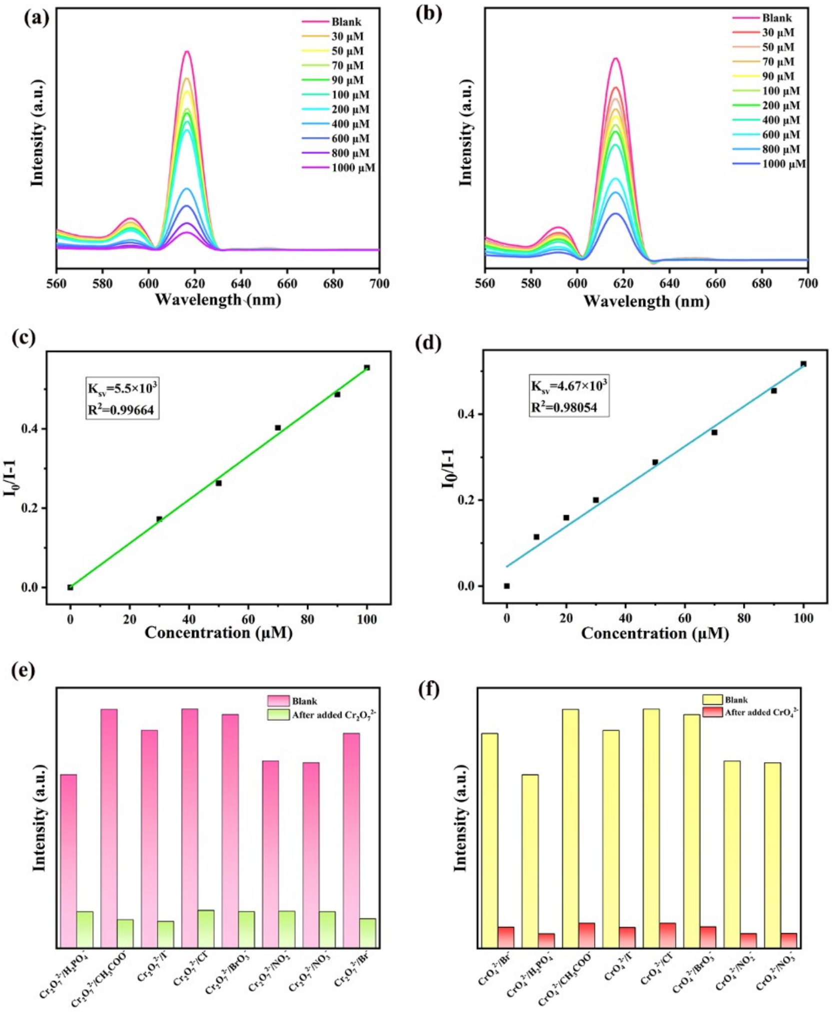

Fig. S11 Fluorescence spectra of **CUST-924** in $Cr_2O_7^{2-}$ (a) and CrO_4^{2-} (b) aqueous solutions from 0 to 1000 μM. Stern-Volmer plots of **CUST-924** in aqueous solutions of $Cr_2O_7^{2-}$ (c) and CrO_4^{2-} (d) Study on the anti-interference effect of **CUST-924** on $Cr_2O_7^{2-}$ (e) and CrO_4^{2-} (f) in water in the presence of different anions.

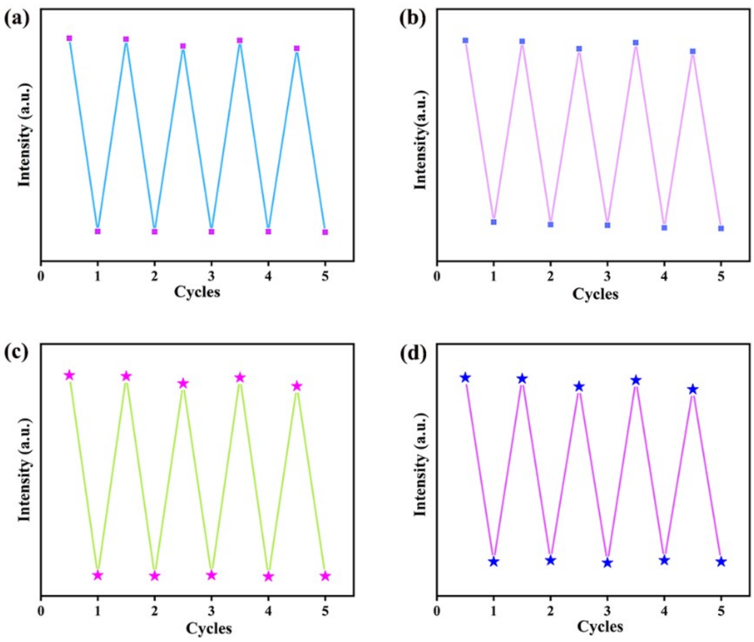

Fig. S12 The recyclability test of **CUST-923** after detecting $Cr_2O_7^{2-}$ (a) and CrO_4^{2-} (b) The recyclability test of **CUST-924** after detecting $Cr_2O_7^{2-}$ (c) and CrO_4^{2-} (d).

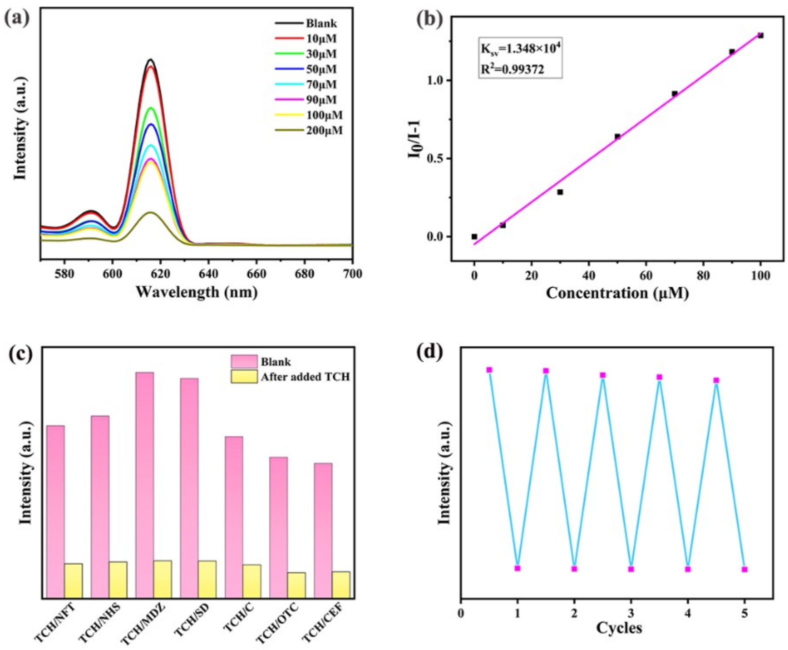

Fig. S13 (a) Concentration-dependent luminescence spectra of **CUST-924** toward TCH in aqueous solution. (b) Stern-Volmer plot of **CUST-924** for TCH. (c) Anti-interference study of **CUST-924** in water against TCH in the presence of different cations. (d) The recyclability test of **CUST-924** after sensing TCH.

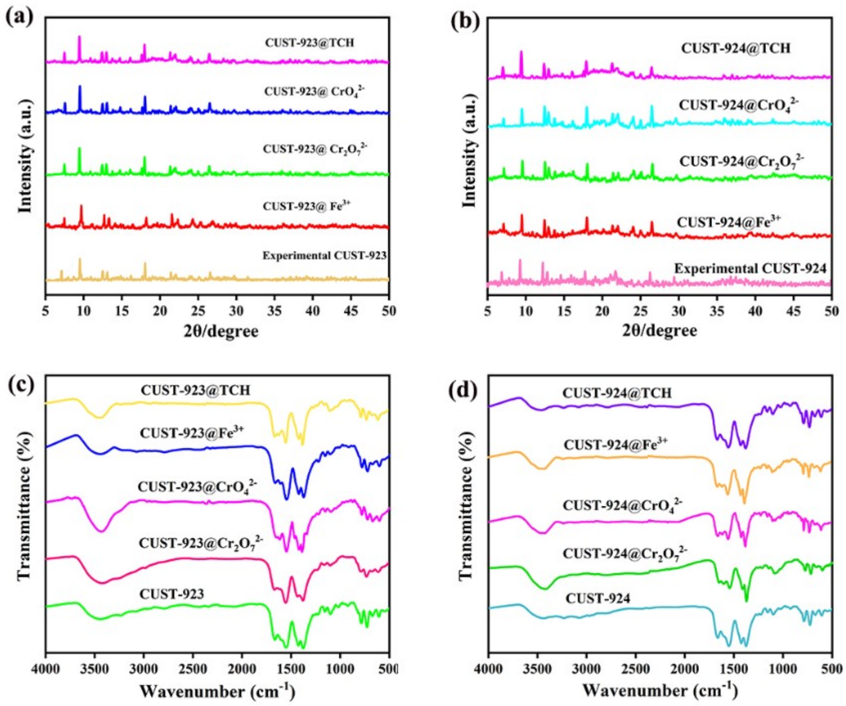

Fig. S14 PXRD patterns of **CUST-923** (a) and **CUST-924** (b) After storage Fe^{3+}, $Cr_2O_7^{2-}$, CrO_4^{2-}, TCH. IR spectra of **CUST-923** (c) and **CUST-924** (d) in different solutions.

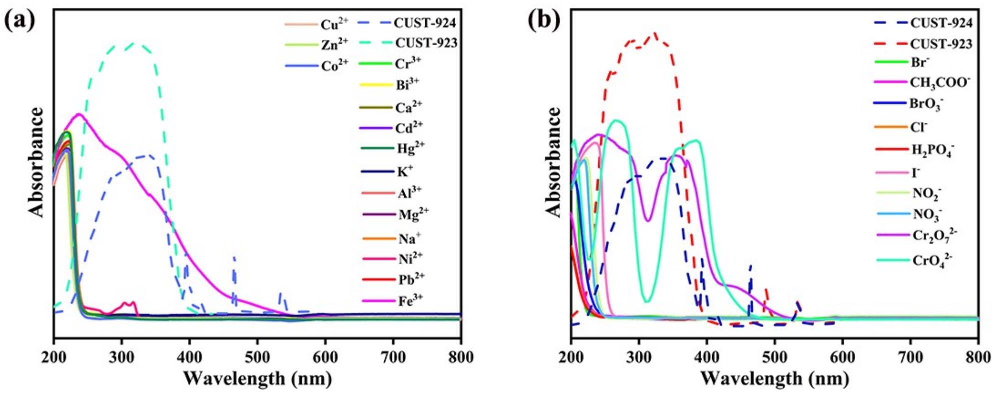

Fig. S15 The excitation spectra of **CUST-923** (a) and **CUST-924** (b) overlap with the absorption spectra of different solutions.

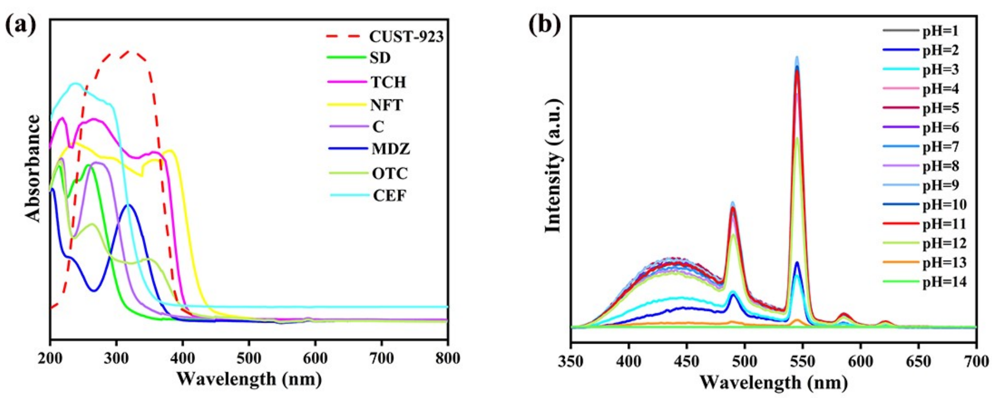

Figure S16 (a) The excitation spectra of **CUST-923** overlap with the UV absorption spectra of different antibiotic solutions. (b) Fluorescence intensity of **CUST-923** at different pH.

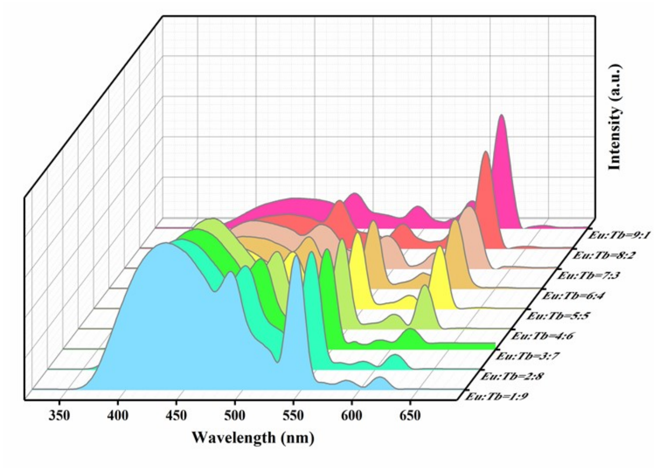

Fig. S17 Solid state fluorescence emission spectra of Eu_xTb_{1-x}-PDAI with different doping ratios.

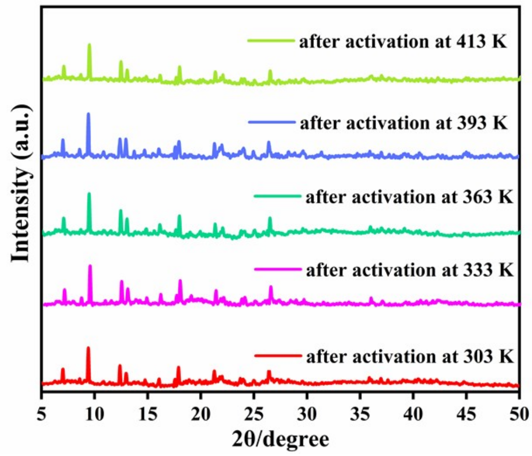

Fig. S18 PXRD patterns of $Eu_{0.1}Tb_{0.9}$-PDAI after activation at 303 K - 413 K.

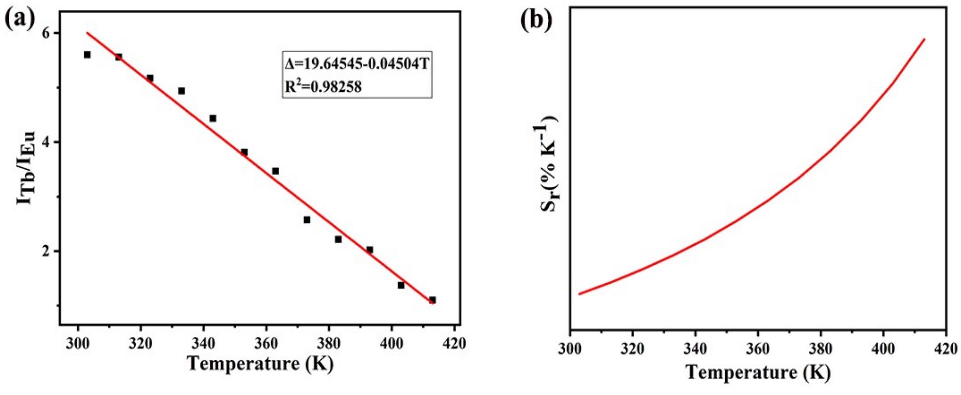

Fig. S19 (a) Fitted curves of the integrated intensity ratio for $Eu_{0.1}Tb_{0.9}$-PDAI. (b) Relative sensitivity of $Eu_{0.1}Tb_{0.9}$-PDAI.

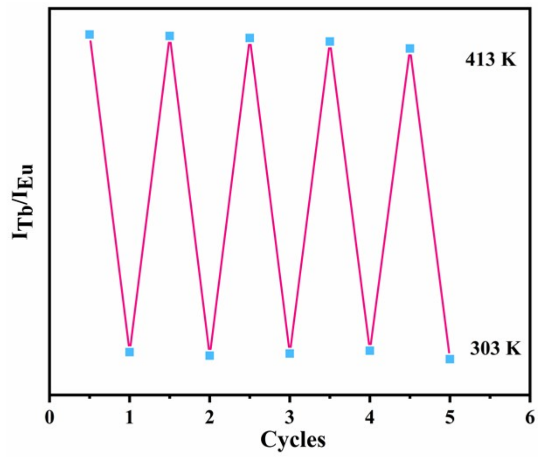

Fig. S20 Cyclic temperature measurement experiments of $Eu_{0.1}Tb_{0.9}$-PDAI.

References

S1 S. Srivastava, V. Kumar, R. Gupta, *Cryst Growth Des*, 2016, **16**, 2874-2886.

S2 X. Wen, C. Xin, W. Zhang, C. Ding, Z. Li, *J Lumin*, 2023, **263**, 120092.

S3 X. Yu, A. A. Ryadun, D. I. Pavlov, T. Y. Guselnikova, A. S. Potapov, V. P. Fedin, *Angew Chem Int Edit*, 2023, **62**, e202306680.

S4 X. Yu, A. A. Ryadun, K. A. Kovalenko, T. Y. Guselnikova, V. G. Ponomareva, A. S. Potapov, V. P. Fedin, *Dalton T*, 2023, **52**, 8695-8703.

S5 F. Zhong, C. Li, Y. Xie, H. Xu, J. Gao, *J Solid State Chem*, 2019, **278**, 120892.

S6 N. Wu, H. Guo, X. Wang, L. Sun, T. Zhang, L. Peng, W. Yang, *Colloid Surface A*, 2021, **616**, 126093.

S7 F. Y. Ge, G. H. Sun, L. Meng, S. S. Ren, H. G. Zheng, *Cryst Growth Des*, 2019, **20**, 1898-1904.

S8 S. Chen, Z. Shi, L. Qin, H. Jia, H. Zheng, *Cryst Growth Des*, 2017, **17**, 67-72.

S9 Z. J. Lin, H. Q. Zheng, H. Y. Zheng, L. P. Lin, Q. Xin, R. Cao, *Inorg Chem*, 2017, **56**, 14178-14188.

S10 F. Y. Ge, G. H. Sun, L. Meng, S. S. Ren, H. G. Zheng, *Cryst Growth Des*, 2019, **20**, 1898-1904.

S11 J. Liu, S. Liu, J. Ma, Y. Diao, M. Li, J. He, Q. Zhang, *Inorg Chem*, 2020, **59**, 17884-17888.

S12 S. R. Zhang, W. T. Zhang, X. Li, G. J. Xu, W. Xie, Y. H. Xu, Z. M. Su, *Inorg Chem*, 2025, **64**, 2990-2999.

S13 C. S. Cao, H. C. Hu, H. Xu, W. Z. Qiao, B. Zhao, *Cryst Growth Des*, 2016, **18**, 4445-4451.

S14 W. H. Yao, X. G. Mu, C. Y. He, Y. H. Zhang, *J Mol Struct*, 2023, **1289**, 135886.

S15 J. Luo, Y. Lin, J. Yang, C. Xu, *Phys Scripta*, 2024, **99**, 065566.

S16 B. Parmar, Y. Rachuri, K. K. Bisht, R. Laiya, E. Suresh, *Inorg Chem*, 2017, **56**, 2627-2638.

S17 Y. Fu, R. Zhang, P. Lv, F. Chen, W. Xu, *J Solid State Chem*, 2022, **306**, 122724.

S18 Y. Yin, J. Zhang, C. Ji, Z. Zhao, X. Wang, P. Wang, Y. Yang, *Talanta*, 2025, **294**, 128200.

S19 H. Wang, J. Xu, D. S. Zhang, Q. Chen, R. M. Wen, Z. Chang, X. H. Bu, *Angew. Chem. Int. Ed.*, 2015, **54**, 5966-5970.

S20 Y. Yang, Y. Wang, Y. Feng, X. Song, C. Cao, G. Zhang, W. Liu, *Talanta*, 2020, **208**, 120354.

S21 W. N. Miao, B. Liu, H. Li, S. J. Zheng, H. Jiao, L. Xu, *Inorg Chem*, 2022, **61**, 14322-14332.

S22 S. Wang, J. Jiang, Y. Lu, J. Liu, X. Han, D. Zhao, C. Li, *J. Lumin*, 2020, **226**, 117418.

S23 P. V. Alekseevskiy, X. Yu, A. S. Efimova, N. A. Zhestkij, Y. A. Mezenov, Y. A. Kenzhebayeva, V. A. Milichko, *Laser & Photonics Reviews*, 2025, 2401912.